JOURNAL OF THERMOPHYSICS AND HEAT TRANSFER
Vol. 8, No. 4, Oct.–Dec. 1994

Radiation Transport Calculation in High Enthalpy Environments for Two-Dimensional Axisymmetric Geometries

T. H. Gogel,* M. Dupuis,† and E. W. Messerschmid‡
University of Stuttgart, D-70550 Stuttgart 80, Germany

A Monte Carlo method to determine radiative source terms and boundary heat fluxes for generic, two-dimensional axisymmetric geometries was developed. For the geometrical discretization, curvilinear structured grids have to be used. Thus, it is possible to use essentially the same grid as for the initial flowfield computation. The spectral behavior of gas radiation was considered as well as thermochemical nonequilibrium conditions of the medium using the NEQAIR code system. The radiation process is simulated by a large number of energy-carrying bundles emitted at the appropriate locations, having the appropriate wavelength and direction of emission. These bundles are then traced on their path through the computational domain and their spectral absorption behavior is calculated. Departing from a given flowfield solution for the considered geometry, the radiation simulation method is initiated and yields the radiative source terms in an adequate form for coupling with the energy equations of the flowfield. The iteration is performed in a loosely coupled manner. A first radiation assessment for the case of a trajectory point of the ROSETTA-re-entry is presented.

I. Introduction

RADIATION transport may not be neglected for applications dealing with high enthalpy environments such as plasma wind tunnels, electric spacecraft propulsion, and atmospheric re-entry with superorbital velocities. In order to couple the radiation transport term with flowfield computations for these applications, a spatially resolved computation of this term is necessary. Caused by the complexity of the physics involved for absorptive, spectrally resolved calculations of radiation transport, mostly one-dimensional approximation methods are published in the literature using the infinite slab approximation. The results obtained are then valid only for the stagnation region and are only marginally applicable for the implementation into flowfield codes.

To overcome this shortcoming and to achieve a fully two-dimensional axisymmetric method, the development of a Monte Carlo simulation of reabsorptive, spectrally resolved radiation transport was undertaken by Keefer and Gogel.[1] The objective was to determine the radiative heat flux in the constrictor region of an arcjet using ammonia as propellant. This problem was still one dimensional in the sense that only a radial variation of the temperature profile and no variation in axial direction in the cylindrical constrictor region was used. Furthermore, local thermodynamic equilibrium (LTE) was assumed for the calculation of absorption and emission coefficients.

Since 1991, this method was extended to enable a fully two-dimensional axisymmetric radiation calculation for spacecrafts entering Earth's atmosphere with superorbital velocities. Data bases for air as they are available from the literature[2,3] were implemented, and the second one, the NEQAIR, was modified to fulfill the need of a Monte Carlo simulation. The objective of this work is to develop the computational tools to compute the coupled flow-radiation field around vehicles like the European "ROSETTA" capsule.

Thus, a two-dimensional axisymmetric method to compute absorptive, spectrally resolved radiation transport yielding the spatially resolved total radiation source term and the radiation heat fluxes across the boundaries of the computational domain was developed. In connection with Park's data base NEQAIR,[4] this calculation can be done for flowfields in chemical and thermal nonequilibrium.

II. Description of the Method

The total energy equation for a viscous, compressible, reacting, and radiating gas can be written as[5]

$$\frac{\partial}{\partial t}E + \nabla Hv = \nabla\bar{\tau}v + \nabla\lambda\nabla T + \nabla\lambda_v\nabla T_v + \nabla\lambda_e\nabla T_e + \nabla\sum_s H_s D_s \nabla\psi_s - \nabla\cdot q_r \tag{1}$$

On the left side the derivative of the total energy E with respect to time and the convective term, with the total enthalpy H, is given. On the right side the viscous terms, the heat fluxes for the heavy particle translational degree of freedom (DOF), described by the temperature T, the contribution of the vibration of the molecules, described by the temperature T_v, and the heat flux in the electron gas, given in terms of the electron temperature T_e, and the mass diffusion contributions, expressed with the species enthalpies H_s, effective diffusion coefficients D_s, and mole fractions ψ_s, are given. The coupling between radiation and flow energy is incorporated by the total radiation source term $\nabla\cdot q_r$. This term also appears in the electron energy equation.

This complex term can be determined with a Monte Carlo method using the transport equation[6]

$$\nabla\cdot q_r = 4\pi\varepsilon - \int_0^\infty \int_{4\pi} a_\lambda I_\lambda \, d\omega \, d\lambda \tag{2}$$

The first term on the right side represents the emission behavior with ε being the total emission coefficient, the second term on the right side describes the absorbed power with the absorption coefficient a_λ and the intensity I_λ. In this term, an integration of the incoming radiation intensity over the entire computational domain is necessary, accomplished by integrating over the entire solid angle 4π, which is a difficult task to be done using more abstract mathematical or numerical

Presented as Paper 93-2804 at the AIAA 28th Thermophysics Conference, Orlando, FL, July 6–9, 1993; received Aug. 30, 1993; revision received March 21, 1994; accepted for publication April 4, 1994.

*Research Engineer, Institut für Raumfahrtsysteme. Member AIAA.
†Student, Aerospace Engineering. Student Member AIAA.
‡Professor, Director Institut für Raumfahrtsysteme.

simulation methods. A direct simulation of this process is possible by using discrete, energy-carrying radiation bundles that are emitted in a physically consistent way. This represents the transition from a Euler to a Lagrange description of the problem; instead of the determination of the incoming radiation in a volume element out of its surroundings, single radiation-carrying bundles are traced from their location of emission on their way through the computational domain.

The simulation process is performed as follows. The region of interest is discretized. Therefore, a structured grid of the flowfield computation can be truncated by just using each second or fourth grid line in order to stay within memory or run-time limits for the radiation calculation. Next, emission and absorption coefficients are calculated and stored for each volume element. Using an LTE assumption, the emission coefficient may be obtained by derivation from absorption coefficients and Kirchhoff's law, for the more general nonequilibrium case they are determined accordingly in the NEQAIR data base. Now, total emission in a volume element located at the axial coordinate x and radial coordinate z is obtained by using

$$\frac{dQ}{dV}(x, z) = 4\pi \int_{\lambda=0}^{\infty} \varepsilon_\lambda \, d\lambda \tag{3}$$

The emission coefficient $\varepsilon_\lambda = \varepsilon_\lambda(\lambda, p, T, T_v, T_e, \psi_i)$ is a function of the thermodynamic state, determined by the temperatures T, T_v, T_e, the pressure p, and the mole fractions ψ_i of all species i at the location x, z. It is calculated using an appropriate data base. This represents the emission term already in the transport Eq. (2). The integration over the solid angle to obtain total values is included in Eq. (3). For the Monte Carlo simulation, appropriate distribution functions have to be calculated. A general introduction is given in Refs. 7 and 8. The distribution function $P_\lambda(p, T, T_v, T_e, \psi_i)$ for the radiation wavelength is defined as[1,8]

$$P_\lambda(p, T, T_v, T_e, \psi_i) = \frac{\int_{\lambda^*=0}^{\lambda} \varepsilon_\lambda \, d\lambda^*}{\int_{\lambda=0}^{\infty} \varepsilon_\lambda \, d\lambda} \tag{4}$$

This is a normalized function that yields the probability of the wavelength of an emitted photon to be less than or equal to λ for a given thermodynamic state. This function will be used to determine the wavelength of a radiation bundle using a random number r_λ with $0 \le r_\lambda \le 1$. Such a random number represents the ordinate of the function P_λ for a single emission event, and the wavelength of the emission is given by the respective abscissa value. The spectrum is adequately simulated by using a large number of bundles and equally distributed random numbers in the interval [0, 1]. The actual number of bundles to be used depends on the specific spectrum to be simulated as well as on the accuracy requirements of the sought after solution.

The total emitted radiation Q_{tot} in the computational domain is obtained by integrating over all grid volume elements:

$$Q_{tot} = \int \int_V \int \frac{dQ}{dV} \, dV \tag{5}$$

Each bundle carries an energy increment of

$$\Delta Q = Q_{tot}/n_{tot} \tag{6}$$

with n_{tot} being the user specified total number of bundles. The number of bundles emitted out of each volume element, labeled j is

$$n_j = \mathrm{INT}\left(\frac{dQ_j}{Q_{tot}} + 0.5\right) \cdot n_{tot} \tag{7}$$

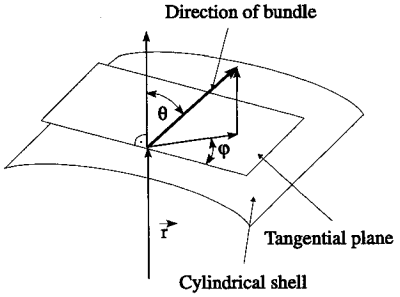

Fig. 1 Description parameters for bundle direction.

with dQ_j being the power emitted from the volume element, and INT signifies the integer operation.

For each volume element the total number of bundles emanating is determined and the simulation process can be initiated.

The direction of a radiation bundle is determined by the cone angle θ and the azimuthal angle φ, as sketched in Fig. 1. For each bundle, these angles are determined using two random numbers r_θ and r_φ

$$\theta = \arccos(1 - 2r_\theta) \tag{8}$$

$$\varphi = 2\pi r_\varphi \tag{9}$$

These expansions are given by Siegel and Howell[8] for the modeling of isotropic radiation, so that the emission is equally distributed over the entire solid angle. These angles remain constant along the path of a radiation bundle, since refraction is neglected in this work.

Another random number r_l is used to describe the absorption behavior of a bundle. The following expansion is used:

$$\ln r_l = -\int_0^l a_\lambda(s) \, ds \tag{10}$$

Here, $a_\lambda(s)$ is the spectral absorption coefficient along the path s of the bundle. The integration is replaced by a summation in the discretized computational grid. In a volume element crossed by a bundle, the pathlength Δs covered by this bundle in this volume element must be determined. The spectral absorption coefficient must also be known and is predetermined for all volume elements in an adequate spectral resolution with the data base. The bundle is considered to be absorbed in a volume element, if the right side of Eq. (10) becomes smaller than the left side in this volume element. The energy balance of this volume element is then increased by the energy increment carried by the bundle [Eq. (6)]. It is evident that this term yields a strong spectral dependence and that special care must be taken to appropriately resolve the spectral features in the data base. Again, for a large number of radiation bundles the exponential absorption behavior as required by the underlying physics is simulated by this procedure.[8]

Using the above-mentioned four random numbers, each radiation bundle is characterized. It then has to be traced from its location of emission on its way through the computational domain. Therefore, a ray-tracer was developed. The determination of the source term is then done by bookkeeping in each volume element of both emitted and absorped bundles.

A. Development of a Ray-Tracer

As mentioned above, each bundle has to be traced on its path through the curvilinear computational grid after its wavelength, direction of emission, and absorption parameter were determined. The same grid as for a previous flowfield computation may be used, which should be truncated to stay within reasonable storage and run-time requirements. Three possible cases have to be considered:

1) The bundle is absorbed in the volume element. Its energy is deposited in this volume element. The tracing of the bundle is terminated.

2) If the volume element is a boundary element and the bundle leaves via a boundary surface, the appropriate counter for the boundary heat fluxes has to be increased, the tracing of the bundle is terminated.

3) If the bundle traverses the element and is not considered to be absorbed, the index of the next element on its path as well as the surface element through which it enters this element has to be determined for the further tracing of this bundle.

These tasks are performed using a "ray-tracer," which was developed in accordance with methods used in computer graphics.[9] It was developed for two-dimensional axisymmetric geometries. It calculates intersections of the ray with the boundary surfaces of each volume element, which may be cones, cylinders, or planes. The pathlength covered within a volume element Δs can be determined from the intersections. A number of integer operations are also performed to determine the entry and exit surface of the bundle and the index of the volume element to be crossed next by the bundle.

The absorption coefficient in accordance with the bundle wavelength is determined in each volume element in order to perform the calculation indicated in Eq. (10). Thus, the spectral character of the absorption is taken into account.

It should be mentioned that the direction of the bundles is considered fully three dimensional as given in Eq. (11), merely the volume elements are considered to be two-dimensional axisymmetric, annular elements through which the rays are passing. this limits the application of the developed method on two-dimensional axisymmetric geometries.

Mathematically, the bundle is described as a ray in parametric form:

$$\begin{bmatrix} x \\ y \\ z \end{bmatrix} = \begin{bmatrix} x_0 \\ y_0 \\ z_0 \end{bmatrix} + t \cdot \begin{bmatrix} a \\ b \\ c \end{bmatrix} \tag{11}$$

Herein, x is the axial coordinate, and y and z are two perpendicular base vectors in the azimuthal plane. The point (x_0, y_0, z_0) is the point of origin of the ray, e.g., the center of the emitting cell, a, b, c are the coordinates of the directional vector, and t is a pathlength parameter, which is directly identical to the covered pathlength in case of normalized directional vectors. The directional vectors are obtained from the bundle's direction defined in Eqs. (8) and (9) using

$$a = \sin(\theta)\cos(\varphi) \tag{12}$$

$$b = \sin(\theta)\sin(\varphi) \tag{13}$$

$$c = \cos(\theta) \tag{14}$$

These are directional cosines, so that the directional vector is normalized. Boundary surfaces in a grid may be planes perpendicular to the z axis, and the calculation of the intersection with a ray Eq. (11) is straightforward. The two other possible boundary surfaces, cones, or cylinders, are quadratic surfaces whose intersections with the ray can be found using the quadratic formula. The difference between the parameter t of entry and exit surface of the volume element under consideration is the needed pathlength of the bundle covered within the element Δs.

B. Random Numbers

The quality and smoothness of a solution determined with a Monte Carlo method is dependent on the quality of the random numbers that are used. These numbers are not random numbers in the true sense of the word, since they are determined using deterministic algorithms. The numbers are created in the interval [0, 1]. Two kinds of random-number generators were compared: 1) pseudo- and 2) quasirandom numbers. For the first kind, a suitable code is given in Ref. 10. It is based on nested linear congruential generators, which yield random numbers with an infinite period. Using these numbers, stochastic concentrations of numbers can be detected.

A quasirandom number generator, as given in Ref. 11, is based on Sobol-sequences creating evenly distributed numbers in the interval. Thus, the disadvantage of the pseudorandom numbers is removed. This generator is designed for stochastic multidimensional cases.

The quasirandom number generator for the two-dimensional directional parameters and the one-dimensional implementation for the wavelength distribution and the absorption parameter, respectively, were determined to be effective. Treating all parameters simultaneously with four-dimensional quasirandom numbers was not successful, since the deterministic pattern for a coarse resolution gives rise to a biased spectral distribution of wavelengths.

A comparison of both random-number generators is given in Ref. 12. The basic result was that for a given amount of radiation bundles, the result obtained with the quasirandom numbers is smoother than the result using pseudorandom numbers. Thus, it is better suited for coupling with a flow computation. However, special care must be taken to avoid the problem caused by the deterministic patterns mentioned above. More parametric studies with a variation of the spectral resolution will be done in the future to investigate the random number generator or combination of random number generators that give the most consistent result.

III. Adaption of a Data Base

An adequate data base had to be implemented into the Monte Carlo procedure. First, calculations were made for the case of arc columns in high-pressure air and ammonia.[1] Therefore, the absorption data were precalculated for a set of temperatures for the given pressures and stored in data files. For the calculated LTE cases, the emission coefficient was inferred using Kirchoff's law. These files were used as input values for the calculation. Next, the RAD/EQUIL code of Nicolet[2] was used. The original LTE version was employed, therefore, it was limited to LTE calculations. Hartung's extended version for nonequilibrium calculations[13] was not available for this work. Then the NEQAIR code of Park in the published version of 1985[3,4] was adapted into the code system. Since these codes are used to precompute absorption and emission data before the Monte Carlo simulation is initiated, they are also refered to as a "data base" in this context. A short description of the NEQAIR code is given below. The improved version developed by Moreau et al.[14] was not available for this work.

The NEQAIR was developed to calculate radiative properties of nonequilibrium air in the low-density regimes expected during the flight of aeroassisted, orbital transfer vehicles. From the given nonequilibrium thermodynamic state variables, the code calculates number densities of internal states and the accompanying emission and absorption characteristics.

A description of the underlying theory, which is briefly outlined here, is given by Park.[3,15] The computer code is described in Ref. 4. The code is written in standard FORTRAN and is structured in modular form. Therefore, the implementation in a radiation transport code is relatively straightforward.

The temperatures describing the thermal nonequilibrium are the heavy particle translational temperature T (assumed to be equal to the rotational temperature of the molecules), vibrational temperature T_v, and the electron temperature T_e. Thus, the modeling coincides with the one commonly used for the calculation of nonequilibrium flows and, therefore,

these data are readily available from most computer programs for the calculation of nonequilibrium flows.

The spectra emitted by atoms and molecules of air are modeled as follows[3,15]: Atomic radiation consists of the line radiation of N and O, the free-free and free-bound continua. The molecular radiation consists mostly of the first negative system of N_2^+, the first positive and the second positive systems of N_2, the beta and gamma systems of NO and the Shumann-Runge system of O_2. The lack of ionic lines is justified by their irrelevance at temperatures below about 12,000 K. Above this temperature the radiation is underestimated. To incorporate possible ablation products, the violet and red systems of CN may exist and are implemented into the code.

First, in the NEQAIR code the assumption of equal electron and electronic temperature is revoked. This assumption is only valid for the two low-lying states of atoms and O_2 molecules. In the radiation calculation, these low-lying states do not participate.[15] Instead, radiation emanates from high electronic states. Therefore, one must solve for the number densities of all electronic states from first principles. Since electronic excitation rates are fast, the quasi-steady-state assumption is generally valid for electronic states. Since the vibrational temperature T_v and the rotational-translational temperature T are assumed to be given, the population of vibrational and rotational states within an electronic states of the molecules can be determined.

To perform the calculation, the three temperatures mentioned above, T, T_v, T_e, and the number densities of all species involved must be known.

In the first step, one determines the wavelengths of the various radiation mechanisms under consideration. To do so, the energy levels of the upper and lower states of each radiating mechanism have to be calculated. The necessary data are given in a data file. These are the energy levels of the atoms and the rotational and vibrational constants of the molecules. After the determination of the energy levels of the latter constants, the radiation wavelength λ is calculated using the difference between the two energy levels, $\Delta E = h\nu = hc/\lambda$.

In the second step, the intensity factor is calculated. For an atomic line, this is simply Einstein's A coefficient. For a molecule, it is given in terms of the electronic transition moment and the Frank-Condon factors. A more complete description is given by Park.[15] For the free-bound and free-free continua, it is given in terms of absorption cross sections.

In the third step, the distribution of intensity over wavelength is determined. For an atomic line, one first determines the shape of the line over the wavelength. This shape is considered to be a Lorentzian line shape plus a Gaussian line shape caused by Doppler broadening, the blend being a Voigt profile. The molecular band radiation is implemented on a line-by-line basis, each line shape being determined as for the atomic lines. For the continua, appropriate formulas have been incorporated into the code. The intensity calculation is done for both emission and absorption coefficients independently using an excitation temperature for each transition, as required by the nonequilibrium environment. These three steps and the calculation of the number densities of the electronically excited states are performed in the NEQAIR code.

As was pointed out above, the choice of frequency incrementation is crucial. In the NEQAIR, the wavelength interval under consideration, which is given in terms of the low and high boundary wavelength in the input file, is divided into a user-specified amount of frequency intervals with equal separation. Thus, the incrementation is the same for all points in the domain to be calculated. However, it is then somewhat arbitrary, especially with respect to the narrow nitrogen resonance line, to get a good representation of atomic lines. This is a major drawback for the Monte Carlo calculation that can be corrected in the original version only by choosing a narrow incrementation in order to catch all the lines. For the example case given below, the results for $\nabla \cdot \boldsymbol{q}_r$ varied by more than an order of magnitude for different spectral resolution using the original NEQAIR. A new incrementation technique should be developed, with similar features as the method used by Nicolet[2] or Hartung.[13]

Here, two measures were taken to improve the atomic line representation. These reduced the spectral resolution dependence of the result for the example case given to below 3%, once more than 3000 points of spectral resolution were used. For less than 3000 points in the wavelength range as given below, again, significant variations of the results with wavelength occurred.

As a first step, to obtain the maximum absorption that is at the line center, these values as given in the data file are lumped to the closest point of the wavelength grid that is determined first. The error occurring caused by this slight shift of the line centers is negligible for the chosen resolution (e.g., 5000 points in the interval from 800 to 8000 Å). Second, if a linewidth $\delta_{1/2}$ (being the full width at half maximum) is found to be in the order of the grid spacing $\Delta\lambda$, $0.3\delta_{1/2} \leq \Delta\lambda$, then the line is additionally resolved using 11 points, that is the point at the centerline and 5 points on either side of the line.

An example is given in Fig. 2. The emission coefficient of the nitrogen resonance triplet of the transition array $2p^3 - 2p^2(^3P)3s$ is depicted for the equilibrium condition at T = 14,000 K and p = 1 bar, values representative of the postshock conditions of the ROSETTA-re-entry case that will be presented later. The overall resolution, as used by the NEQAIR, was 5000 points in the interval from 800 to 8000 Å. Additional storage was necessary to store the fine structure of the lines. The wavelength points as given in the original NEQAIR are marked by crosses and the values are connected by a dashed polygon. The atomic lines after the modification for a better resolution of atomic lines is depicted as a solid line polygon, the calculated values are marked by circles. It is obvious that an adequate distribution function, Eq. (4), can only be obtained using the improved resolution. Also, the absorption behavior that exhibits the same line shape is only consistent through this modification. Furthermore, it can be seen that for this triplet, being representative for all strong resonance multiplets, a slight shifting of the line centers to the adjacent points in the wavelength discretization does not affect the overall shape since these lines overlap only in the far wings.

The most time critical part of the calculation is the determination of the molecular bands. The time for this calculation is larger by a factor of about 10 as compared to the calculation of atomic and continuum radiation. As compared to the RAD/EQUIL, the run-time per spectrum is increased by a factor

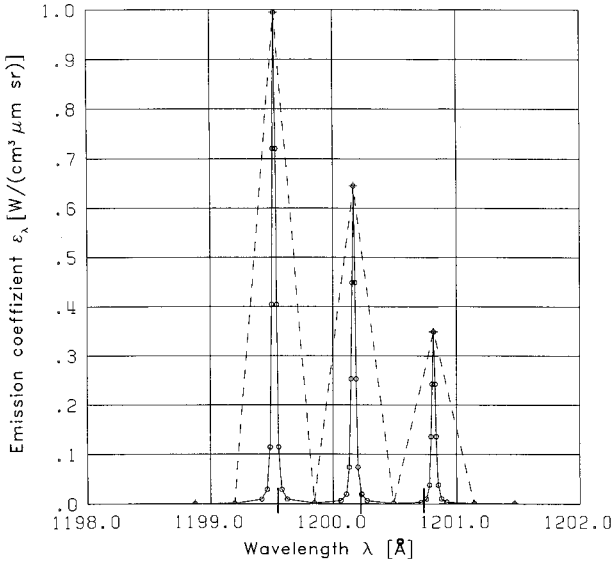

Fig. 2 Nitrogen triplet at T = 14,000 K, p = 1 bar.

of about 8. In the NEQAIR, each molecular band is principally resolved into its rotational lines within the vibrational-electronic transitions. However, these features are too fine to be adequately represented by the available version of the NEQAIR code to enable an accurate Monte Carlo simulation: for a typical application case, as given below, the minimum spectral resolution to be used in the NEQAIR is in the order of 3000 points to simulate a wavelength range of 800–8000 Å. Additional memory has to be provided to store the highly resolved atomic lines, as described above. For other application cases, the upper wavelength boundary must be extended to include atomic lines that might become significant, thus the resolution becomes even coarser. Since two arrays, 1) the distribution function and 2) the absorption coefficient, have to be stored for each grid point, it is apparent that the spectral resolution is limited by the memory available in the computer. The objective of this work was to calculate the example case described below on an IBM RISC 6000/320H with 64 MB memory. To achieve this, less than 4000 points had to be used to simulate the spectrum with the NEQAIR. Since the incrementation in the NEQAIR is done with equal frequency intervals rather than clustering points around narrow spectral features, it is evident that a line-by-line representation of molecular bands cannot be adequately resolved. The application case presented below is dominated by the atomic line radiation, the molecular radiation is negligible. Therefore, the influence of the coarse resolution of the molecular bands has to be assessed in the future using a molecular radiation dominated (usually high altitude, low density) application case.

A "smeared band" model of molecular radiation, as it was adopted by Hartung,[13] is better suited for a broadband radiation transport calculation. The error introduced by this continuous variation of absorption and emission coefficients is acceptable under most conditions where molecular radiation is significant. The development of such a smeared band model can be found in Ref. 16.

IV. Example Calculation

A number of verification calculations were done since the program system was developed. First, two application cases for arc discharges were calculated using a basic code version. Details are published in Ref. 1. The extension of the method to a fully two-dimensional axisymmetric version was then verified using the same application cases. After the implementation of each data base (RAD/EQUIL and NEQAIR), verification calculations were performed using different application cases and the results obtained were compared to those given by other authors, e.g., Carlson and Gally.[17] However, experimental validation of the code with any of these data bases is still pending. Here, one sample result for an application case using the NEQAIR as data base is presented. The result shows the application on a superorbital velocity entry of the ROSETTA capsule. The nonequilibrium flowfield solution was calculated using a thermochemical nonequilibrium code developed described in Ref. 18. Another such solution, including ablation species in the boundary layer, was calculated using the code described in Ref. 19. This code will be used for further development of the radiation code system.

Depicted is the translational temperature distribution for a trajectory point at an altitude of h = 56 km and a velocity v = 12.9 km/s (Fig. 3). The postshock pressure is about 1 bar, as can be seen in Fig. 3. The chemical composition along the centerline can be seen in Fig. 4. The flowfield is essentially in thermal equilibrium, a small chemical nonequilibrium region exists behind the shock. The original flowfield grid (73 lines axial, 41 lines radial) was reduced by a factor of 2 for the radiation calculation. Thus, the total storage requirement could be reduced to 48 MB for the radiation calculation, and an IBM RISC-Station 6000/320H with 64 MB memory could be used for the initial test calculations. For the last run, whose result is presented here, an IBM RISC 6000/550 was used.

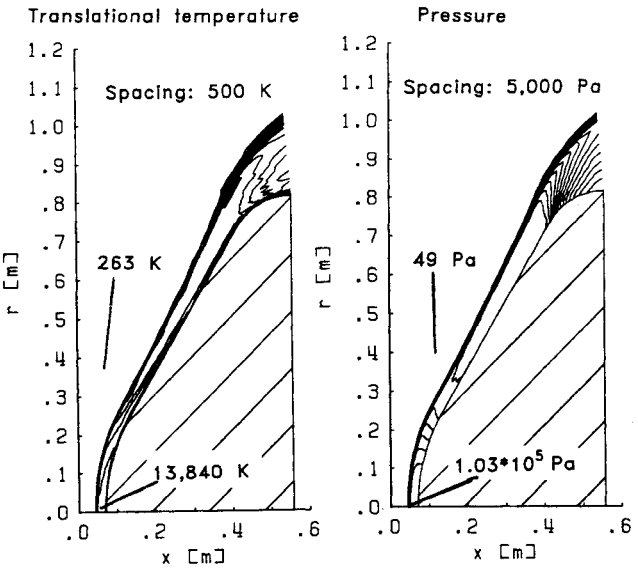

Fig. 3 Translational temperature and pressure distribution.

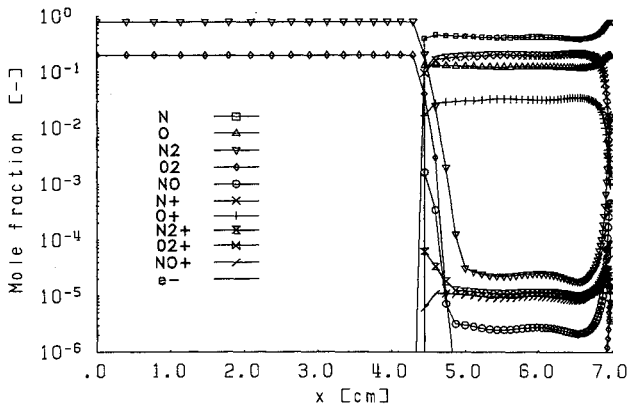

Fig. 4 Chemical composition along centerline.

The spectra were resolved using n_s = 3500 points basic resolution in the interval from 800 to 8000 Å, an additional 1000 points had to be used for the resolution of the narrow atomic lines. The chosen wavelength interval contains almost the entire radiation for this example case. This was found after an additional run with a much larger interval, the result being larger by only 2%. A total of n_{tot} = 12,000,000 bundles was used for this run. The run-time was 7140 s on an IBM RISC 6000/550. This large number of bundles was necessary since this case is optically thick and most of the bundles were absorbed immediately in their cell of origin. Since such events do only require one pass of the ray-tracer, that is in the cell of origin itself, the effect on run-time is not significant. However, to obtain a smooth result a still significant number of bundles must be emitted in spectral regions being not optically thick. Previous runs were performed using 3,000,000 bundles to assess the accuracy of the method. This result exhibits still a significant roughness, but the resulting radiative heat flux on the wall stays within an error band of less than 5% of the result as obtained with the large number of bundles.

Figure 5 shows the divergence term of the radiative heat flux. Since this case is optically thick, the solution needs to be smoothed using a digital filter to remove unphysical peaks. This term can now be coupled into the flowfield computation, which will be the next step. Next, Fig. 6 depicts the radiative heat flux along the vehicle wall, labeled $q_{r,w}$. A radial dependence can be clearly seen, justifying a two-dimensional calculation. The convective heat fluxes, as computed using the thermochemical implicit non-equilibrium alogrithm (TINA),[13] including the ablation species in the boundary layer, are also depicted, they are labeled $q_{c,w}$. It is obvious that for

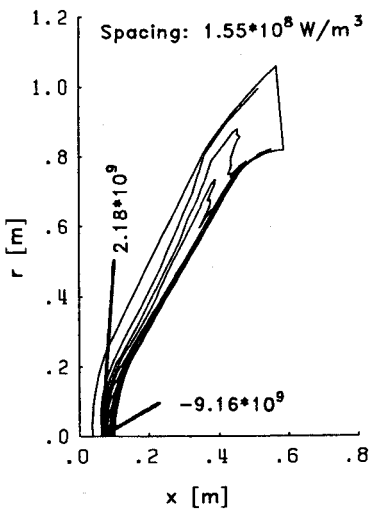

Fig. 5 Radiative source term $\nabla \cdot q_r$.

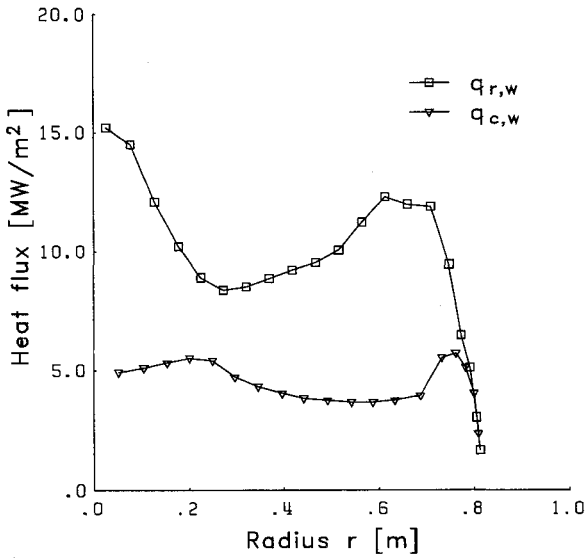

Fig. 6 Heat fluxes along vehicle wall.

this application case the radiative flux is the dominant heating mechanism for the vehicle wall, underlining the necessity to compute this energy transport mechanism. As compared to the stagnation point radiative flux as given in the equilibrium radiative heating tables,[20] this result is lower than the four values defining the parametric boundaries in these tables. Using the interpolation procedure with the density as an independent variable, the result of $q_{r,\text{stag}} = 15$ MW/m² presented here is about a factor of 2 lower than the interpolated value of $q_{r,\text{inter}} = 29.9$ MW/m². However, this result was based on a two-dimensional Navier-Stokes solution of the flowfield, and therefore included the cold, absorbing boundary layer that was not the case for the one-dimensional calculation used in Ref. 20. Furthermore, since the exact postshock conditions were not specified in Ref. 20, a direct comparison with the values used here could not be made. An iteration with the flowfield code has not yet been performed.

Figure 7 depicts the emission coefficient at a location on the stagnation streamline behind the shock. It clearly shows the dominance of the atomic line radiation for this application case as well as molecular band structures and the continuum part.

It was found that about 94% of the radiative flux in the stagnation region emanates from a wavelength below 2000 Å. The most significant emission contribution is from the nitrogen resonance lines mentioned before, which are carrying more than 50% of the total emission. Since these lines exhibit

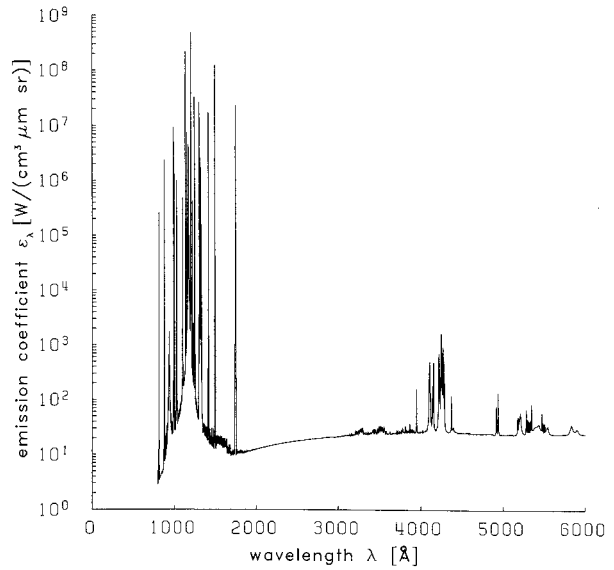

Fig. 7 Postshock emission coefficient.

a strong self-absorption, their participation to the overall radiation transport is not as significant as their emission contribution. An accurate assessment of the influence of the boundary layer on the radiative heat transfer has not yet been undertaken.

V. Conclusions

The development of a Monte Carlo method for the computation of gas radiation for two-dimensional axisymmetric geometries has been reported. The modifications necessary to the NEQAIR data base were described. Spectral features, especially the atomic lines, were adapted for use with the Monte Carlo method. A result using a Navier-Stokes solution of the flowfield and the NEQAIR code as data base for the radiation calculation is described. The stagnation point result is compared to stagnation point radiative heat fluxes of other authors using one-dimensional approximations and an inviscid flow model. The agreement was satisfactory considering the differences in the calculation methods.

The results obtained with the developed method are the spatially resolved radiative source term suitable for coupling into a flowfield code and radiative fluxes across the boundaries of the computational domain. Coupled flow-radiation field computations will be done in the future.

In order to reduce run-time and storage requirement, further changes—especially of the data base—are necessary. The smeared band approximation for the molecular bands should be used and multiplets of the high series atomic lines should be represented by their parent line. To obtain a more versatile data base also applicable for plasma flow simulation, ionic lines should be implemented.

The method will be parallelized on a workstation cluster. This method is especially suited for parallelization, since the radiation bundles used for the simulation are not influencing each other.

Acknowledgments

This work was supported by Fluid Gravity Engineering Ltd., United Kingdom, with the ESA/ESTEC Contract 9397/91/NL/FG of the ESA study program "Aerochemistry Effects in Hypersonic Flows." The method was initiated at the University of Tennessee Space Institute under the supervision of D. Keefer. Parts of the preliminary studies and the development of the flowfield code were supported by the Deutsche Forschungsgemeinschaft in the frame of the collaborative research project SFB 259 "Hochtemperaturprobleme rückkehrfähiger Raumtransportsysteme" established at the Uni-

versity of Stuttgart, Stuttgart, Germany. The authors are greatly indebted for the support.

References

[1]Gogel, T. H., Sedghinasab, A., and Keefer, D. R., "Calculation of Arcjet Constrictor Plasma Temperatures Using a Monte Carlo Method for Radiation Transfer," AIAA Paper 90-2615, July 1990.

[2]Nicolet, W. E., "Advanced Methods for Calculating Radiation Transport in Ablation-Product Contaminated Boundary Layers," NASA CR-1656, Sept. 1970.

[3]Park, C., "Calculation of Nonequilibrium Radiation in the Flight Regimes of Aeroassisted Orbital Transfer Vehicles," *Thermal Design of Aeroassisted Orbital Transfer Vehicles*, Vol. 96, Progress in Astronautics and Aeronautics, AIAA, New York, 1985, pp. 395–418.

[4]Park, C., "Nonequilibrium Air Radiation (NEQAIR) Program: User's Manual," NASA-TM-86707, July 1985.

[5]Gnoffo, P. A., Gupta, R. N., and Shinn, J. L., "Conservation Equations and Physical Models for Hypersonic Air Flows in Thermal and Chemical Nonequilibrium," NASA TP 2867, 1989.

[6]Anderson, J. D., *Hypersonic and High Temperature Gas Dynamics*, McGraw-Hill, New York, 1989.

[7]Hammersley, J. M., "Monte Carlo Methods," Methuen and Co., Ltd., London, 1964.

[8]Siegel, R., and Howell, J. R., *Thermal Radiation Heat Transfer*, Hemisphere, New York, 1980.

[9]Hanrahan, P., "A Survey of Ray-Surface Intersection Algorithms," *An Introduction to Ray Tracing*, edited by A. S. Glassner, Academic Press, London, 1989.

[10]Press, W. H., Flannery, B. P., Teukolsky, S. A., and Vetterling, W. T., "Numerical Recipes, the Art of Scientific Computing," Cambridge Univ. Press, Cambridge, England, UK, 1988.

[11]Press, W. H., and Teukolsky, S. A., "Quasi- (that is, Sub-) Random Numbers," *Computers in Physics*, Vol. 3, No. 6, 1989, pp. 76–79.

[12]Döngi, F. L., "Erweiterung einer Monte Carlo-Methode zur zweidimensionalen, spektralen Simulation des Strahlungsenergieflusses in Hochenthalpieströmungen," Diplomarbeit IRS 91-S 26, Institut für Raumfahrtsysteme, Univ. Stuttgart, Stuttgart, Germany, 1991.

[13]Hartung, L. C., "Development of a Nonequilibrium Radiative Heating Prediction Method for Coupled Flowfield Solutions," AIAA Paper 91-1406, June 1991.

[14]Moreau, S., Laux, C. O., Chapman, D. R., and MacCormack, R. W., "A More Accurate Nonequilibrium Air Radiation Code: NEQAIR Second Generation," AIAA Paper 92-2968, July 1992.

[15]Park, C., *Nonequilibrium Hypersonic Aero-thermodynamics*, Wiley, New York, 1990.

[16]Zel'dovich, Y. B., and Raizer, Y. P., "Physics of Shock Waves and High-Temperature Hydrodynamic Phenomena," Academic Press, New York, 1966.

[17]Carlson, L. A., and Gally, T. A., "Effect of Electron Temperature and Impact Ionization on Martian Return AOTV Flowfields," *Journal of Thermophysics and Heat Transfer*, Vol. 5, No. 1, 1991, pp. 9–19.

[18]Gogel, T., "Numerische Modellierung von Hochenthalpieströmungen mit Strahlungsverlusten," Dissertation, Universität Stuttgart, Institut für Raumfahrtsysteme, Stuttgart, Germany, 1994.

[19]Netterfield, M. P., "Validation of a Navier-Stokes Code for Thermochemical Non-Equilibrium Flows," AIAA Paper 92-2878, July 1992.

[20]Sutton, K., and Hartung, L. C., "Equilibrium Radiative Heating Tables for Earth Entry," NASA TM 102652, May 1990.